Available online at www.sciencedirect.com

Journal of Applied Research and Technology

CCADET CENTRO DE CIENCIAS APLICADAS Y DESARROLLO TECNOLÓGICO

Journal of Applied Research and Technology 13 (2015) 543–550 www.jart.ccadet.unam.mx

Original

A laser spectroscopy system with combined absorption, polarization rotation and fluorescence detection to study two photon transitions in atomic rubidium

Oscar López-Hernández [a], Santiago Hernández-Gómez [a], Francisco Sebastián Ponciano-Ojeda [a], Cristian Mojica-Casique [a], Ricardo Colín-Rodríguez [a], Jesús Flores-Mijangos [a], Daniel Sahagún [b], Fernando Ramírez-Martínez [a,*], José Jiménez-Mier [a]

[a] *Instituto de Ciencias Nucleares, Universidad Nacional Autónoma de México, Circuito Exterior s/n, Ciudad Universitaria, Del. Coyoacan, México, D.F., CP 04510, Mexico*

[b] *Instituto de Física, Universidad Nacional Autónoma de México, Circuito Exterior s/n, Ciudad Universitaria, Del. Coyoacan, México, D.F., CP 04510, Mexico*

Received 28 March 2015; accepted 18 September 2015
Available online 19 November 2015

Abstract

The design and construction of an experimental system for studying two photon spectroscopy processes in atomic rubidium is presented. It is designed to measure absorption and polarization rotation induced by any of the two laser beams and also the visible fluorescence that results from decay of the excited states. Two home-built diode lasers are used to produce the optical fields that later interact with room temperature rubidium atoms. Using counterpropagating beams allows velocity selection of the groups of atoms that interact with both laser beams. The system was tested in the 5 S → 5 $P_{3/2}$ → 5 D_j ladder energy level configuration of atomic rubidium. Blue fluorescence (420 nm) that results from decay of the intermediate 6P_j states is filtered and then measured with a photomultiplier tube. Absorption and fluorescence spectra provide mutually complementary information about the interaction between the rubidium atoms and the two optical fields.

Keywords: Laser spectroscopy; Two-photon transition; Rubidium

1. Introduction

High-resolution laser spectroscopy free of Doppler broadening has made substantial progress through the study of the interaction between two optical fields and an atomic medium, such as an alkali metal vapor. This progress has also brought improvement in laser stabilization techniques that are commonly used in atom manipulation such as laser cooling and trapping (Metcalf & Van der Straten, 1999). The combination of precisely controlled experiments and the development of theoretical models is a key factor in the advance of high-resolution laser spectroscopy. The agreement between experiment and theory is quite satisfactory under many experimental circumstances (Harris et al., 2006; Himsworth & Freegarde, 2010; Noh, Moon, & Jhe, 2010; Pearman et al., 2002; Smith & Hughes, 2004). For the purposes of this article, one can broadly classify the experiments that use atomic transitions induced by two photons in two groups. In the first one, the effect of the light atom interaction is observed in the modification of the light as it is transmitted through the atomic medium (Auzinsh, Budker, & Rochester, 2010). There are changes in both absorption and polarization of a probe light beam as it passes through an atomic medium interacting with optical fields. In the second group of experiments, the light produces excited states in the atoms that can be detected, for instance, by looking at the atomic fluorescence. In these experiments one measures the atomic population in the excited states. The 5 S → 5 D_j two-photon excitation in atomic rubidium provides very good examples of both types of experiments. Absorption of a probe beam in the 5 S → 5 $P_{3/2}$ → 5 $D_{5/2}$ stepwise

* Corresponding author.
E-mail address: ferama@nucleares.unam.mx (F. Ramírez-Martínez).
Peer Review under the responsibility of Universidad Nacional Autónoma de México.

http://dx.doi.org/10.1016/j.jart.2015.09.006

excitation allows the study of electromagnetically induced transparency (EIT) in a Doppler broadened medium (Badger, Hughes, & Adams, 2001; Drampyan, Pustelny, & Gawlik, 2009; Fulton, Shepherd, Moseley, Sinclair, & Dunn, 1995; Gea-Banacloche, Li, Jin, & Xiao, 1995; Li, Jin, & Xiao, 1995; McGloin, Dunn, & Fulton, 2000; Moon, Lee, & Kim, 2005; Moon & Noh, 2011a, 2011b; Noh & Moon, 2012; Sargsyan, Bason, Sarkisyan, Mohapatra, & Adams, 2010; Sargsyan, Sarkisyan, Krohn, Keaveney, & Adams, 2010; Wielandy & Gaeta, 1998; Xiao, Li, Jin, & Gea-Banacloche, 1995). Examples of fluorescence detection in this stepwise excitation are the two-photon experiments performed either with a single frequency or two different frequencies (Hamid, Çetintaş, & Çelik, 2003; Nez, Biraben, Felder, & Millerioux, 1993, 1994; Ryan, Westling, & Metcalf, 1993; Sanguinetti, Mure, & Minguzzi, 2007; Touahri et al., 1997), electron shelving (Thoumany et al., 2009), frequency up-conversion (Meijer, White, Smeets, Jeppesen, & Scholten, 2006), four wave mixing (Akulshin, McLean, Sidorov, & Hannaford, 2009), direct frequency comb spectroscopy (Marian, Stowe, Felinto, & Ye, 2005). These types of experiments have also been developed for advanced undergraduate laboratories (Jacques, Hingant, Allafort, Pigeard, & Roch, 2009; Olson & Mayer, 2009; Olson, Carlson, & Mayer, 2006). In this work we present a two-photon spectroscopy setup in atomic rubidium in which it is possible to simultaneously detect the absorption and/or rotation of polarization of one of the two excitation light components and the fluorescence of an spontaneous decay channel. Detection of the fluorescence light provides complementary information to the one obtained by performing velocity-selective polarization spectroscopy of room temperature rubidium atoms (Colín-Rodríguez et al., 2015; Flores-Mijangos, Ramírez-Martínez, Colín-Rodríguez, Hernández-Hernández, & Jiménez-Mier, 2014; Hernández-Hernández et al., 2009). This paper is structured as follows. In Section 2 we review the 5 S, 5 $P_{3/2}$, 5 D_j ladder system in atomic rubidium, including the fluorescence decay paths. In Section 3 we present the experimental setup. Details about the construction of our diode lasers and the fluorescence detection system are also given. Examples of experimental spectra obtained with this setup are shown in Section 4. Finally, conclusions are presented in Section 5.

2. The 5 S → 5 $P_{3/2}$ → 5 D_j two-photon transition in atomic rubidium

To understand the different spectroscopy experiments that are performed in our setup we present an energy level diagram of atomic rubidium in Figure 1. The values of the total angular momenta F and hyperfine structure splittings shown here pertain to ^{85}Rb, and a similar diagram can be obtained for ^{87}Rb. In our setup (see below) a continuous wave (CW) diode laser at 780 nm is used to excite room temperature atoms from one of the hyperfine components of the 5 S ground state into the 5 $P_{3/2}$ state (the rubidium D_2 line). A second CW diode laser beam at 776 nm, counterpropagating with the first one, provides a photon for excitation into the 5 D_j (j = 3/2, 5/2) hyperfine manifolds. After this two-step excitation the atoms in the 5 D_j state decay back to the ground state. One of the decay paths is by cascade

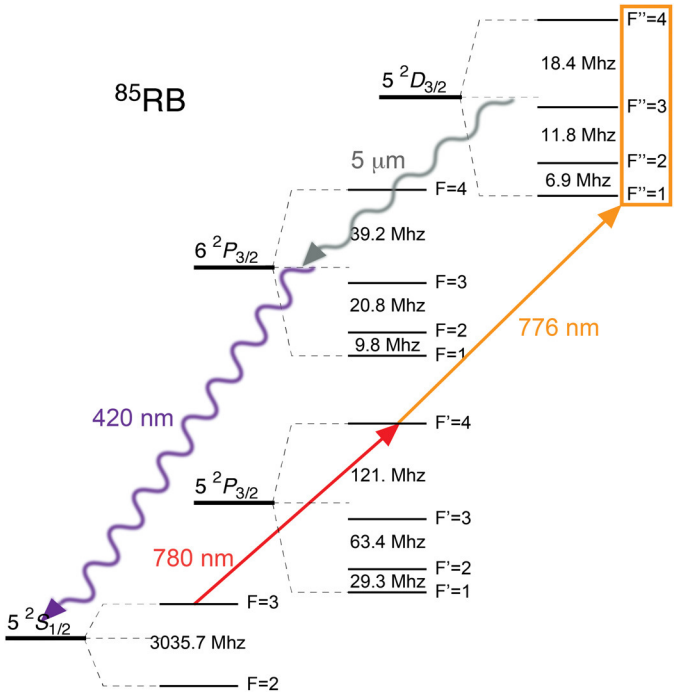

Figure 1. Energy-level diagram for the 5 $S_{1/2}$ → 5 $P_{3/2}$ → 5 $D_{3/2}$ of atomic ^{85}Rb, including the hyperfine states.

emission of an IR photon (5 μm) into the 6 P_j state, followed by emission of a 420 nm photon. Detection of the excitation process can be made by measuring changes in the absorption or rotation of the linear polarization of one of the laser beams (Flores-Mijangos et al., 2014; Hernández-Hernández et al., 2009) or by detection of the emission of a 420 nm fluorescence photon. The hyperfine splitting of the 5 $S_{1/2}$ state in atomic rubidium is larger than the D_2 line Doppler width at room temperature (≈500 MHz). Therefore, the total angular momentum F of the initial step in our excitation ladder is well defined. However, the hyperfine splitting of both 5 $P_{3/2}$ and 5 D_j states is smaller than the D_2 Doppler width. If the frequency of one of the two lasers is fixed, then by scanning the frequency of the second laser one can perform velocity selective (Flores-Mijangos et al., 2014; Hernández-Hernández et al., 2009) spectroscopy resulting in lines that are not broadened by the Doppler effect. The resonant frequency ν_2 and the velocity of the group of atoms that simultaneously interact with both laser beams is given by the solution of the set of equations

$$\nu_a = \nu_1\left(1 - \frac{v}{c}\right)$$
$$\nu_b = \nu_2\left(1 + \frac{v}{c}\right) \quad (1)$$

where ν_a is one of the atomic resonant frequencies of the 5 S → 5 $P_{3/2}$ hyperfine manifold, ν_b is an atomic resonant frequency of the 5 $P_{3/2}$ → 5 D_j manifold and ν_1 is the fixed frequency of one of the lasers. Here it is important to mention that the transitions must be allowed by the electric dipole selection rule $\Delta F = 0, \pm 1$. In our system we use balanced detection to measure the absorption and polarization of the 780 nm beam used in the first step of the excitation. We add a photomultiplier tube to the system

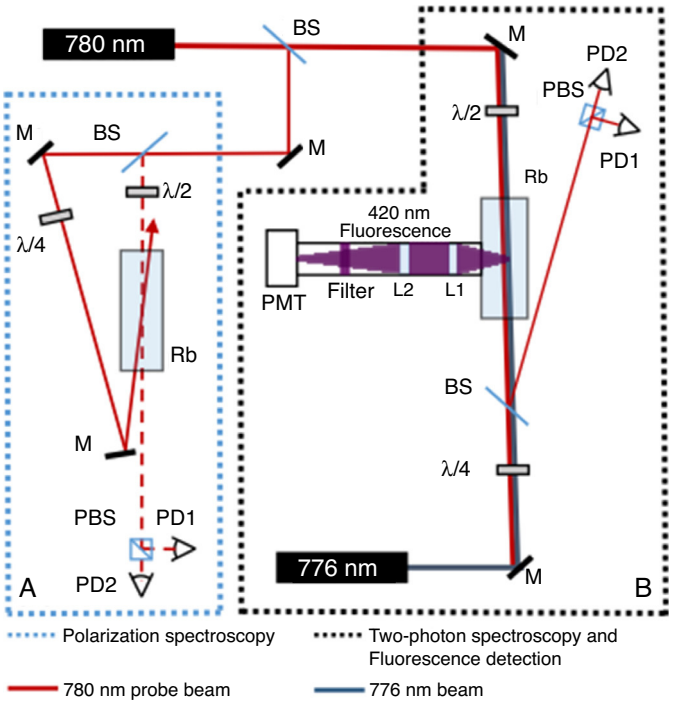

Figure 2. The two-photon spectroscopy setup. (A) Polarization spectroscopy setup for the 780 nm laser (ECDL) (Harris et al., 2006; Pearman et al., 2002). (B) The two-photon spectrometer that includes systems for detecting the absorption and polarization rotation of the 780 nm light component and the 420 nm decay fluorescence. Both 780 nm and 776 nm are external cavity diode lasers (ECDL). λ/2, half wave plate; λ/4, quarter wave plate; PMT, photomultiplier tube; L1 and L2, lenses for fluorescence collection; PD1 and PD2, Si photodiodes; M, mirror; BS, beam splitting glass slide; PBS, polarizing beams splitter cube.

in order to detect emission of 420 nm photons. These measurements of absorption, polarization and fluorescence are made as functions of the frequency of one of the two lasers, with the frequency of the other laser fixed. In one type of experiment the absorption of the 780 nm laser is measured as its frequency is scanned. One then observes the effect of the passively locked 776 nm light component on top of a broad Doppler absorption well. In this configuration one obtains an electromagnetically induced transparency signal (Gea-Banacloche et al., 1995; Olson & Mayer, 2009). In a second type of experiment, polarization spectroscopy (Harris et al., 2006; Pearman et al., 2002) is used to lock the frequency of the 780 nm laser to the maximum $F \rightarrow F+1$ cyclic transition, and the frequency of the 776 nm laser is scanned. In this case one obtains velocity-selective absorption and polarization spectra (Colín-Rodríguez et al., 2015). For these two cases detection of the 420 nm fluorescence emission takes place only when the frequency of the lasers resonantly excites the 5 D_j state for atoms with a specific velocity, and it appears on top of a flat background

3. Experimental setup

The experimental system that was constructed is depicted schematically in Figure 2. Two external cavity diode lasers (ECDL) are used to produce the two-photon transition in an atomic rubidium cell kept at room temperature. The spectrometer is shown in the right hand side box, denoted as (B), of Figure 2. The 780 nm probe beam is linearly polarized, and its polarization direction is controlled with a half waveplate. The 776 nm beam is circularly polarized with a quarter wave plate, and both beams counterpropagate along a commercial rubidium cell (Tryad Technology) mounted inside an ambient light isolation and magnetic field shielding setup. A photomultiplier tube with a filter and lens assembly (see below) is used to detect the fluorescence light. A microscope slide at near normal incidence is used to send part of the probe beam into the balanced detection array after it has crossed through the Rb cell. This setup can therefore register simultaneously both the blue fluorescence detected by the photomultiplier tube and the variations induced in the absorption and direction of polarization of the 780 nm laser component as a result of the interaction of both beams with the atomic medium. Also, a portion of the 780 nm laser is sent to a polarization spectrometer (Harris et al., 2006; Pearman et al., 2002) shown in Figure 2(A). This spectrometer can be used to monitor the frequency of the 780 nm laser when it is scanning, but it can also be used to lock the frequency of this laser when the other laser is scanned. Both diode lasers are based on the Littrow-mount design of Arnold, Wilson, and Boshier (1998). We also include an output mirror that maintains the emission direction fixed (Hawthorn, Weber, & Scholten, 2001). Laser diodes whose nominal emission wavelength is 785 nm (Hitachi HL7851G, 50 mW output power) are mounted in collimating tubes (Thorlabs LT110P-B) containing an aspheric collimating lens ($f = 6.24$ mm, N.A. = 0.40). The collimating tube is fixed to a modified mirror mount (Newport U100-P) in order to provide mechanical stability for the diode. The laser beam then falls onto a holographic, 1800 lines/mm diffraction grating (Edmund NT43-775, 12.7 mm × 12.7 mm × 6 mm). The diffraction grating is fixed with two-sided tape to a 45° wedge so that the first-order diffraction is fed back into the diode. The grating is oriented with its grooves along the vertical direction, and the collimating tube is rotated until the polarization direction of the free-running diode is also vertical. The grating wedge is attached to the L-shaped part of the modified mirror mount (Arnold et al., 1998). Precision screws in the fixed arm of the modified mirror mount provide vertical and horizontal adjustment of the grating, which are used to optimize the grating feedback and also to coarsely tune the emission frequency. Two piezoelectric actuators placed between the horizontal control precision screw and the L-piece are used for scanning of the laser's emission frequency. Control of these piezoelectrics is done via external power sources. The zeroth-order beam from the grating (output beam) is reflected on a broadband dielectric mirror (Newport 05D20BD.2, 12.7 mm in diameter and 3 mm thick), which is mounted on another wedge fixed to the L-piece. This exit mirror fixture is what allows the broad tuning of the laser emission frequency without changing the beam direction (Hawthorn et al., 2001). A thermistor (10 kΩ) placed near the collimating tube is used to measure the laser diode temperature throughout its operation. The modified mirror mount is itself attached to a copper plate that rests on a thermo-electric cooler (Marlow DT-3-2.5) that is used for temperature control. The laser diode current and temperature are set and monitored with

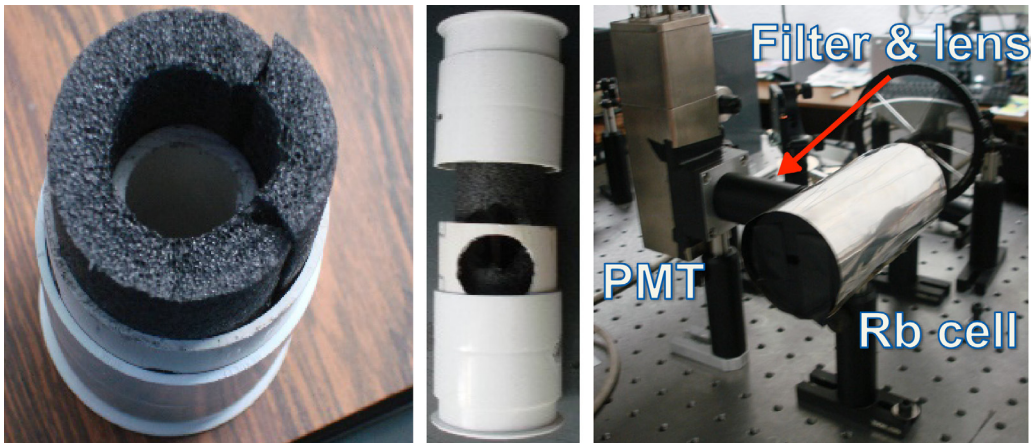

Figure 3. Magnetic field shielding and ambient light isolation setup.

a control card (ILX-Lightwave LDC-3916370) mounted in a multi-card crate (ILX-Lightwave LDC-3908). The two-photon polarization spectroscopy (Carr, Adams, & Weatherill, 2012) and fluorescence detection system are shown in Figure 2(B). As explained above, beams derived from 780 nm and 776 nm ECDLs are superposed in a counter-propagating configuration inside a Rb spectroscopy cell. The 780 nm probe light component is prepared in a linearly polarized state, while the 776 nm pump beam crosses through the cell in a circularly polarized state. In this configuration, optical pumping effects induced by the circularly polarized pump beam create an imbalance in the atomic populations sensed by the two opposing circular polarizations in which the linearly polarized probe beam can be decomposed. This generates a birefringent effect in the absorption of the probe beam. To register this effect, our setup incorporates a glass slide placed at near normal incidence in the path of the probe beam after it has crossed through the Rb cell. The small portion of the beam picked by this slide is in turn registered by a balanced detection system composed by a polarizing beam cube (PBS) and two Thorlabs FDS100 Si photodiodes (PD1 and PD2). A half wave plate ($\lambda/2$) in the path of the probe beam is used to set the direction of the polarization of this beam at a 45° angle with respect to the reflection/transmission axes of the PBS. In this manner, away from resonance the signals registered by the two photodiodes, PD1 and PD2 in (B), are balanced and their difference is equal to zero. On the other hand, when the atomic medium becomes birefringent as a result of its interaction with the two light components, the difference of the signals given by these photodiodes generates dispersion-like signals centered in the atomic two-photon resonances. This setup is particularly useful because the dispersion-like electronic signals generated as a result of the birefringence induced in the atomic medium can be used for locking the frequency of the second laser to transitions in the $5\,P_{3/2} \rightarrow 5\,D_{5/2}$ manifold (Carr et al., 2012). In addition, when the frequencies of the two laser beams are resonant with the two-photon transitions and atoms are successfully pumped into any of the sublevels of the $5\,D_{3/2}$ manifold, as a result of the cascaded spontaneous decay, a visible 420 nm fluorescence signal is produced. Consequently, the spectrometer presented in Figure 2(B) includes a fluorescence detection system optimized for this wavelength. The fluorescence detection system uses a Hamamatsu 1P28 photomultiplier tube (PMT) that has a spectral response ranging from 185 to 650 nm with its maximum sensitivity at 340 nm. To operate the PMT we utilize the high voltage source of a Pacific Precision Instruments photometer (model 110) and a Keithley Instruments, model 428-PROG, programmable current amplifier. To reduce the amount of noise entering into our detection system and to separate the fluorescence from the intense near-infrared excitation light components, the response wavelength bandwidth of the PMT is restricted by means of a band-pass interference filter (CVI Laser Optics F10-420.0-0-1.00, $\lambda_c = 420$ nm, FWHM $= 10 \pm 2$ nm). To characterize and optimize the operation of the PMT and filter combination for the detection of fluorescence with wavelengths ~420 nm, the PMT was mounted on the output port of the Acton Spectra-Pro 2150i spectrometer replacing the near-infrared InGaAs detector originally attached to it. A white LED was then used to measure the spectral response of the PMT. Standard phosphorus-based LEDs start emitting radiation at wavelengths slightly above 400 nm and stop at around 750 nm; on the other hand, the PMT response starting as low as 185 nm is perfectly capable of detecting the lower end of the LED emission and cuts down the spectrum for wavelengths above 650 nm. The blue filter was then placed in the light entrance port of the PMT mount and a transmission spectra with a FWHM of approximately 7 nm centered in 421 nm was measured. This measurement shows that the filter has practically zero transmittance below 412 nm and above 430 nm, which is consistent with the information provided by the manufacturer of the filter. Therefore, the combination of the PMT and blue filter constitutes an excellent system for isolating the 420 nm fluorescence light from the near-infrared excitation light components and to reduce ambient light contributions out of the region of interest. To reduce ambient light contributions in the fluorescence detection system even further, particularly within the high transmission region of the filter, and to shield the atoms from stray magnetic fields, the Rb cell in which the two-photon interaction occurs was mounted inside the house-made holder as shown in Figure 3. The cell is first wrapped in a layer of μ-metal, then covered by a 1/2″ thick layer of black

pipe insulation foam and all this is held inside a section of 2″ in diameter standard plastic tubing. A second layer of μ-metal is added around the tube and the extremes of the resulting cylinder are closed by caps. Holes in the center of these caps allow the excitation laser beams to cross through the cell but restrict as much as possible the entrance of light from the room. A 1″ transverse aperture on the side of this setup and coinciding with the longitudinal center of the cell allows for the attachment of a 1″ Thorlabs lens tube. This tube includes a pair of lenses for collecting the fluorescence light and concentrating it onto the photocathode of the PMT. Finally, the blue filter is located in the piece that attaches the end of the lens tube to the mount of the PMT. The two-photon spectroscopy system incorporates the polarization spectroscopy setup (Harris et al., 2006; Pearman et al., 2002) shown in block (A) of Figure 2. This setup also includes a balanced detection system composed of a polarizing beam splitter cube and two photodiodes for measuring the rotation of the polarization vector of a weak laser light component (dashed line in Fig. 2(A)) when interacting with a Rb vapor in the presence of a more intense, circularly polarized and counter-propagating beam derived from the same laser source. A small portion of the 780 nm light is then also sent into this section of the system that allows us to identify the hyperfine transitions and crossovers in the D_2 line of atomic rubidium and to lock the 780 nm laser to a given transition or cross-over feature of the D_2 line of Rb.

4. Results and discussion

To demonstrate the operation of the laser spectroscopy system, in this section we show spectra recorded by means of the two-photon spectroscopy system described in Section 3 and shown schematically in Figure 2. The spectra presented in Figures 4 and 5 were recorded with the 780 nm laser locked to the 5 $S_{1/2}$, F = 3 → 5 $P_{3/2}$, F′ = 4 cycling transition of ^{85}Rb while the frequency of the 776 nm laser was scanning across the resonances of the 5 $P_{3/2}$ → 5 $D_{3/2}$ manifold. The graph in Figure 4 corresponds to the signal generated in the 420 nm fluorescence detection system. The top and bottom plots in Figure 5 are respectively the rotation of the polarization and the changes in the absorption induced in the probe beam as a result of the presence of the pump beam. The top plot is obtained by taking the difference between the signals recorded by the two photodiodes of the balanced detection system included in our two-photon spectroscopy setup. On the other hand, the absorption signal corresponds to the sum of the signals recorded by these photodiodes. Voigt profile fits of the fluorescence resonances shown in Figure 4 indicate full widths of 6.8 MHz for any of the observed lines. This result is consistent with considering that the width of the lines is limited by the linewidth of the ECDLs utilized in this experiment, which have been independently measured to be of the order of 5 MHz. The performance of our lasers is currently limited by noise in the current supplied to the diodes, but ultra-low-noise current supplies nowadays commercially available could be used to lift this limitation and obtain the width of the resonant two-photon transition. Considering solely transitions allowed by the electric dipole selection rules

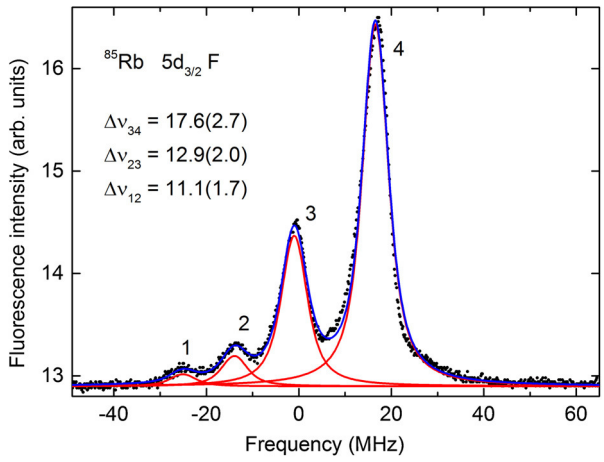

Figure 4. The fluorescence signal obtained with the 780 nm laser locked to the 5 $S_{1/2}$, F = 3 → 5 $P_{3/2}$, F′ = 4 cycling transition of ^{85}Rb and the frequency of the 776 nm laser scanning across the resonances of the 5 $P_{3/2}$ → 5 $D_{3/2}$ manifold. The separation of the peaks is consistent with the hyperfine structure of the 5 $D_{3/2}$ state. The two dominating features (F″ = 4, 3) correspond to atoms with zero velocity component along the direction of propagation of the excitation beams and being excited through the 5 $P_{3/2}$, F′ = 4 sublevel. Velocity groups of atoms moving in the direction of the 780 nm beam are resonant with the 5 $S_{1/2}$, F = 3 → 5 $P_{3/2}$, F′ = 3, 2 transitions and can then be pumped into the 5 $D_{3/2}$, F″ = 2, 1 sublevels.

starting from the 5 $P_{3/2}$, F′ = 4 sublevel, it would be expected to observe only resonances at the frequencies of the F′ = 4 → F″ = 4 and F′ = 4 → F″ = 3 transitions. These are indeed the two dominating contributions that can be identified in all the recorded

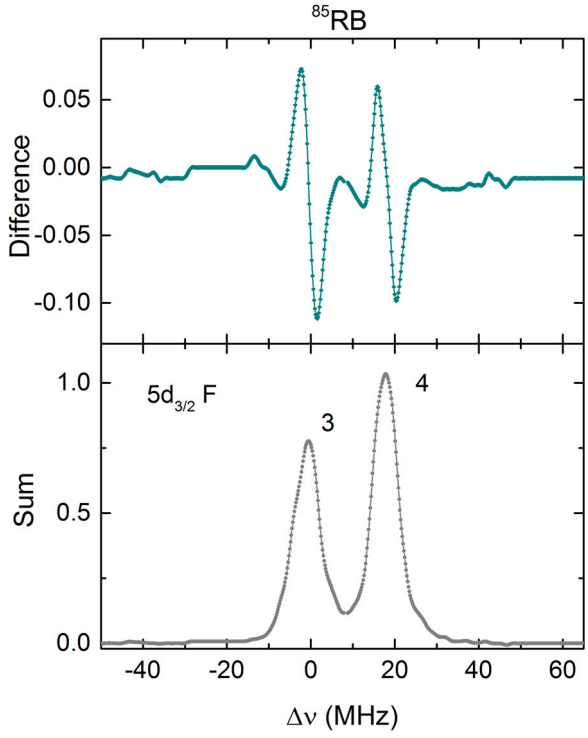

Figure 5. The polarization rotation (top) and the changes in the total absorption (bottom) induced in the 780 nm beam obtained with the 780 nm laser locked to the 5 $S_{1/2}$, F = 3 → 5 $P_{3/2}$, F′ = 4 cycling transition of ^{85}Rb and the frequency of the 776 nm laser scanning across the resonances of the 5 $P_{3/2}$ → 5 $D_{3/2}$ manifold.

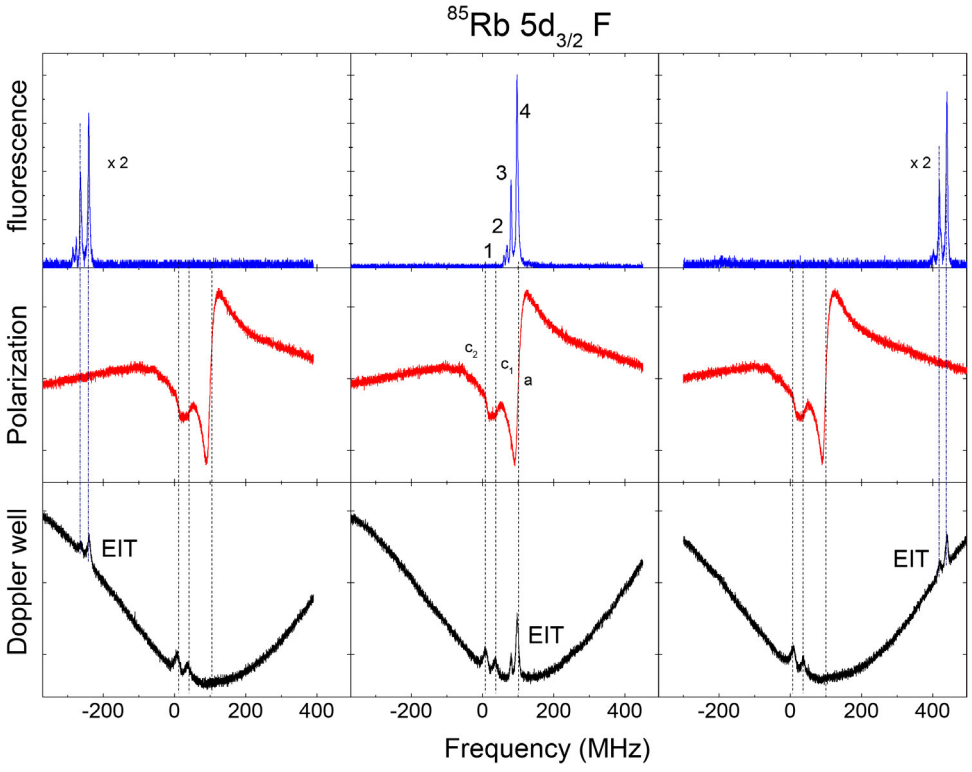

Figure 6. Fluorescence (top) and absorption (bottom) signals obtained with the 780 nm laser scanning across the Doppler broadened D2 line of ^{85}Rb and the frequency of the 776 nm laser passively stabilized to the Doppler shifted resonances of the 5 $P_{3/2} \rightarrow 5\ D_{3/2}$ manifold. The dispersion in the middle panel corresponds to the one-color polarization spectroscopy shown in block (A) of Figure 2. Saturated absorption features in the Doppler well can be identified with the D2 cycling transition (a) and cross-over (c_1 and c_2) features in the one-color polarization spectra. A reduction in the absorption of the 780 nm light is observed whenever the Doppler shifts induced in both light components make a velocity group resonant with the two-photon transitions, producing also a fluorescence signal. Note that the relative height of the four fluorescence peaks depends on the position of these features across the Doppler well.

spectra. However, there are two additional peaks visible only in the fluorescence spectrum. There are groups of atoms for which their velocity component along the direction of propagation of the lasers is such that the Doppler red-shifted frequency of the 780 nm laser beam becomes resonant with the 5 $S_{1/2}$, $F = 3 \rightarrow 5\ P_{3/2}$, $F' = 3$ or even the 5 $S_{1/2}$, $F = 3 \rightarrow 5\ P_{3/2}$, $F' = 2$ transitions. These groups of atoms see the frequency of the 776 nm laser beam shifted to the blue and can then be excited to the $F'' = 2$ and $F'' = 1$ sublevels of the 5 $D_{3/2}$ state. Consequently, the two main peaks in the fluorescence spectrum and the only two features discernible in the polarization and absorption spectra correspond to the group of atoms whose velocity component along the direction of propagation of the laser beams is zero and for whom the excitation goes through the 5 $P_{3/2}$, $F' = 4$; the feature to the right is caused by atoms reaching the 5 $D_{3/2}$, $F'' = 4$ sublevel, while the lower frequency peaks and dispersion signal correspond to atoms excited to the 5 $D_{3/2}$, $F'' = 3$ state. The two remaining peaks appearing in the low frequency end of the fluorescence signal are respectively generated by atoms moving in the same direction as the 780 nm laser beam with a velocity that is enough for producing a Doppler shift equal to the separation between the $F' = 4$ and $F' = 3$, and the $F' = 4$ and $F' = 2$ hyperfine sublevels of the 5 $P_{3/2}$ state. Due to the closeness of the wavelengths of the two components of excitation light, practically the same shift but in the opposite direction is produced in the frequency of the pump light in the reference frame of these moving atoms. Hence, the frequency separation of the four peaks observed in the fluorescence spectra corresponds to the hyperfine structure of the 5 $D_{3/2}$ state. The linear sections in the middle of the polarization spectra dispersion-like curves are ideal for stabilizing the frequency of the second laser of this two-photon excitation scheme (Carr et al., 2012; Pearman et al., 2002). These signals have been used in our laboratory as the error signals that are fed back to the frequency-controlling element of the 776 nm ECDL (either the laser diode current or the voltage supplied to the piezo actuator) to keep it locked to the atomic resonances. The set of spectra in Figure 6 demonstrates an alternative mode of operation of the system described in this paper for the realization of two-photon spectroscopy experiments with atomic rubidium. In these measurements the 780 nm laser was scanning across the Doppler broadened well corresponding to the D_2 line of ^{85}Rb. The frequency of the 776 nm laser beam is passively stabilized without locking. By means of the voltage supplied to the piezo actuator controlling the angle of the ECDL diffraction grating, it is possible to control the location of the two-photon resonances across the Doppler broadened well, clearly demonstrating the selection of velocities naturally occurring in this physical system. A fluorescence signal is observed whenever the sum of the Doppler shifted frequencies of the two laser components in the reference frame of the moving atoms is such that it corresponds to the frequency difference between the 5 $S_{1/2}$ upper hyperfine sublevel and the 5 $D_{3/2}$ manifold. In order to establish a relative

frequency reference in these measurements, the graphs in the middle of Figure 6 show the signal obtained simultaneously by means of the single-photon polarization spectroscopy system depicted in block (A) of Figure 2. The voltage signal in these plots is therefore proportional to the rotation of the polarization induced in the probe beam (dotted beam path in Figure 2(A)) as a result of the optical pumping effects caused by the intense, circularly polarized and counterpropagating laser beam (Pearman et al., 2002). This is precisely the dispersion-like signal utilized for locking the frequency of this laser to an atomic reference in the measurements shown before. The total absorption induced in the secondary beam of the 780 nm probe scanning laser when crossing through the second Rb cell in the presence of the counterpropagating and circularly polarized 776 nm pump beam is presented in the bottom plots of Figure 6. This absorption of the probe beam in the two-photon polarization spectroscopy setup is given by the sum of the signals registered by the two photodiodes that constitute the balanced detection system. This signal shows that a small amount of probe beam light is retro-reflected by the windows of the spectroscopy cell producing saturated absorption features in the Doppler broadened well. These peaks can therefore be identified with the polarization spectroscopy features of the D_2 line cycling transition and dominating crossovers providing a relative frequency scale for the two-photon spectra. In addition, the absorption profiles show the reduction of the absorption of the first photon of the ladder caused by the excitation of different groups of velocities to the 5 $D_{3/2}$ state, features that are accompanied by fluorescence peaks in the top plots. These plots therefore show the effect of the two-photon excitation processes in the absorption of the 780 nm probe beam together with the fluorescence generated as the excited atoms decay back to the ground state. By tuning the frequency of the pump laser it is possible to select the velocity group of atoms interacting with both laser beams and therefore being pumped into the 5 $D_{3/2}$ state. If the frequency of the 776 nm pump beam is prepared above the 5 $P_{3/2} \rightarrow$ 5 $D_{3/2}$ transitions, atoms that are resonant with the two-photon transition must belong to a velocity group such that the Doppler shift makes them interact with the 780 nm light beam at a frequency that is detuned to the red of the 5 $S_{1/2} \rightarrow$ 5 $P_{3/2}$ zero-velocity resonance. In this case, the two-photon transition signatures appear on the low frequency (left) side of the Doppler well. On the other hand, the two-photon resonance features appear at the high frequency end of the Doppler broadened well when the frequency of the pump beam is lower than the frequency of the 5 $P_{3/2} \rightarrow$ 5 $D_{3/2}$ transitions. Hence, the Doppler shift compensates the detuning of the pump beam by selecting a velocity group that sees the frequency of the probe beam detuned by the same amount but in the opposite direction and then sets both laser components in resonance with the respective transitions. An interesting effect that can be clearly observed thanks to our fluorescence detection system is related to the relative height of the recorded peaks. The relative height of the peaks corresponding to resonances that do not go through the 5 $S_{1/2}$, $F = 3 \rightarrow$ 5 $P_{3/2}$, $F' = 4$ cycling transition depends on the frequency of the pump beam and therefore on the position along the Doppler broadened D_2 line well. The lower the frequency of the 780 nm beam, the closer it gets to the $F = 3 \rightarrow F' = 3, 2$ transitions and the greater the population of the velocity group of atoms being exited via these transitions. Consequently, there is a larger population in the velocity groups that can be pumped into the 5 $D_{3/2}$ state via these excitation paths and therefore contributing to the height of the corresponding peaks. Finally, it is important to emphasize that not all the processes that are clearly visible in the fluorescence spectra do show up in the absorption or in the rotation of the polarization of the probe beam, hence demonstrating the utility of simultaneously registering information of the different processes that constitute the two-photon ladder excitation phenomena.

5. Conclusions

Based on two homemade diode lasers and a photomultiplier tube, we have built a system to perform two-photon laser spectroscopy experiments with room temperature rubidium atoms. The system is designed to measure the absorption and the polarization rotation of the probe laser that are induced by interaction between the atoms and the laser beams. It can also measure the 420 nm fluorescence that results from the decay of the 6 P_j excited state in rubidium. The system was tested with electromagnetically induced transparency and velocity-selective spectroscopy in the 5 $S_{1/2} \rightarrow 5P_{3/2} \rightarrow$ 5 D_j ladder configuration of levels, where one of the decay paths of the 5 D_j states is through the intermediate 6 P_j states. The same fluorescence detection can be used for other excitation processes if the 6 P_j state is part of the decay cascade. A one-color polarization spectroscopy cell is incorporated in the setup, and the polarization spectra allow a direct frequency determination of the absorption or fluorescence spectra. The results show significative differences between absorption and fluorescence spectra, and these differences provide complementary information about the processes that take place in the interaction between two optical fields and a Doppler broadened atomic vapor. The setup presented in this paper is also accessible to advanced undergraduate laboratories.

Conflict of interest

The authors have no conflicts of interest to declare.

Acknowledgements

We want to thank J. Rangel for his help in the construction of our diode lasers. This work was supported by DGAPA-UNAM, México, under projects PAPIIT Nos. IN116309, IN110812, and IA101012, and by CONACyT, México, under projects Nos. 168451 and 168498.

References

Akulshin, A. M., McLean, R. J., Sidorov, A. I., & Hannaford, P. (2009). Coherent and collimated blue light generated by four-wave mixing in Rb vapour. *Optics Express*, *17*(25), 22861–22870.

Arnold, A. S., Wilson, J. S., & Boshier, M. G. (1998). A simple extended-cavity diode laser. *Review of Scientific Instruments*, *69*(3), 1236–1239.

Auzinsh, M., Budker, D., & Rochester, S. (2010). *Optically polarized atoms: Understanding light-atom interactions*. Oxford: Oxford University Press.

Badger, S. D., Hughes, I. G., & Adams, C. S. (2001). Hyperfine effects in electromagnetically induced transparency. *Journal of Physics B: Atomic, Molecular and Optical Physics*, *34*(22), L749.

Carr, C., Adams, C. S., & Weatherill, K. J. (2012). Polarization spectroscopy of an excited state transition. *Optics Letters*, *37*(1), 118–120.

Colín-Rodríguez, R., Flores-Mijangos, J., Hernández-Gómez, S., Jáuregui, R., López-Hernández, O., Mojica-Casique, C., et al. (2015). Polarization effects in the interaction between multi-level atoms and two optical fields. *Physica Scripta*, *90*(6), 068017.

Drampyan, R., Pustelny, S., & Gawlik, W. (2009). Electromagnetically induced transparency versus nonlinear Faraday effect: Coherent control of light-beam polarization. *Physical Review A*, *80*(3), 033815.

Flores-Mijangos, J., Ramírez-Martínez, F., Colín-Rodríguez, R., Hernández-Hernández, A., & Jiménez-Mier, J. (2014). Probe-intensity dependence of velocity-selective polarization spectra at the rubidium D2 manifold and comparison with a rate-equation calculation. *Physical Review A*, *89*(4), 042502.

Fulton, D. J., Shepherd, S., Moseley, R. R., Sinclair, B. D., & Dunn, M. H. (1995). Continuous-wave electromagnetically induced transparency: A comparison of V, Λ, and cascade systems. *Physical Review A*, *52*(3), 2302.

Gea-Banacloche, J., Li, Y. Q., Jin, S. Z., & Xiao, M. (1995). Electromagnetically induced transparency in ladder-type inhomogeneously broadened media: Theory and experiment. *Physical Review A*, *51*(1), 576–584.

Hamid, R., Çetintaş, M., & Çelik, M. (2003). Polarization resonance on S–D two-photon transition of Rb atoms. *Optics Communications*, *224*(4), 247–253.

Harris, M. L., Adams, C. S., Cornish, S. L., McLeod, I. C., Tarleton, E., & Hughes, I. G. (2006). Polarization spectroscopy in rubidium and cesium. *Physical Review A*, *73*(6), 062509.

Hawthorn, C. J., Weber, K. P., & Scholten, R. E. (2001). Littrow configuration tunable external cavity diode laser with fixed direction output beam. *Review of scientific instruments*, *72*(12), 4477–4479.

Hernández-Hernández, A., Méndez-Martínez, E., Reyes-Reyes, A., Flores-Mijangos, J., Jiménez-Mier, J., López, M., et al. (2009). Polarized velocity selective spectroscopy of atomic rubidium using counterpropagating beams. *Optics Communications*, *282*(5), 887–891.

Himsworth, M., & Freegarde, T. (2010). Rubidium pump-probe spectroscopy: Comparison between ab initio theory and experiment. *Physical Review A*, *81*(2), 023423.

Jacques, V., Hingant, B., Allafort, A., Pigeard, M., & Roch, J. F. (2009). Nonlinear spectroscopy of rubidium: An undergraduate experiment. *European Journal of Physics*, *30*(5), 921–934.

Li, Y. Q., Jin, S. Z., & Xiao, M. (1995). Observation of an electromagnetically induced change of absorption in multilevel rubidium atoms. *Physical Review A*, *51*(3), R1754.

Marian, A., Stowe, M. C., Felinto, D., & Ye, J. (2005). Direct frequency comb measurements of absolute optical frequencies and population transfer dynamics. *Physical Review Letters*, *95*(2), 023001.

McGloin, D., Dunn, M. H., & Fulton, D. J. (2000). Polarization effects in electromagnetically induced transparency. *Physical Review A*, *62*(5), 1–6.

Meijer, T., White, J. D., Smeets, B., Jeppesen, M., & Scholten, R. E. (2006). Blue five-level frequency-upconversion system in rubidium. *Optics Letters*, *31*(7), 1002–1004.

Metcalf, H., & Van der Straten, P. (1999). *Laser cooling and trapping, graduate texts in contemporary physics*. New York: Springer.

Moon, H. S., Lee, L., & Kim, J. B. (2005). Coupling-intensity effects in ladder-type electromagnetically induced transparency of rubidium atoms. *JOSA B*, *22*(12), 2529–2533.

Moon, H. S., & Noh, H. R. (2011a). Optical pumping effects in ladder-type electromagnetically induced transparency of $5S_{1/2}$–$5P_{3/2}$–$5D_{3/2}$ transition of 87Rb atoms. *Journal of Physics B: Atomic, Molecular and Optical Physics*, *44*(5), 055004.

Moon, H. S., & Noh, H. R. (2011b). Polarization dependence of double-resonance optical pumping and electromagnetically induced transparency in the $5\ S_{1/2} \rightarrow 5\ P_{3/2} \rightarrow 5\ D_{5/2}$ transition of ^{87} Rb atoms. *Physical Review A*, *84*(3), 033821.

Nez, F., Biraben, F., Felder, R., & Millerioux, Y. (1993). Optical frequency determination of the hyperfine components of the $5\ S_{1/2}$–$5\ D_{3/2}$ two-photon transitions in rubidium. *Optics Communications*, *102*, 432–438.

Nez, F., Biraben, F., Felder, R., & Millerioux, Y. (1994). Erratum: Optical frequency determination of the hyperfine components of the $5\ S_{1/2}$–$5\ D_{3/2}$ two-photon transition in rubidium (Optics Commun. 102 (1993) 432). *Optics Communications*, *110*, 731.

Noh, H. R., Moon, G., & Jhe, W. (2010). Discrimination of the effects of saturation and optical pumping in velocity-dependent pump-probe spectroscopy of rubidium: A simple analytical study. *Physical Review A*, *82*(6), 062517.

Noh, H. R., & Moon, H. S. (2012). Transmittance signal in real ladder-type atoms. *Physical Review A*, *85*(3), 033817.

Olson, A. J., Carlson, E. J., & Mayer, S. K. (2006). Two-photon spectroscopy of rubidium using a grating-feedback diode laser. *American Journal of Physics*, *74*(3), 218–223.

Olson, A. J., & Mayer, S. K. (2009). Electromagnetically induced transparency in rubidium. *American Journal of Physics*, *77*, 116–121.

Pearman, C. P., Adams, C. S., Cox, S. G., Griffin, P. F., Smith, D. A., & Hughes, I. G. (2002). Polarization spectroscopy of a closed atomic transition: Applications to laser frequency locking. *Journal of Physics B: Atomic, Molecular and Optical Physics*, *35*(24), 5141–5151.

Ryan, R. E., Westling, L. A., & Metcalf, H. J. (1993). Two-photon spectroscopy in rubidium with a diode laser. *JOSA B*, *10*(9), 1643–1648.

Sanguinetti, S., Mure, E., & Minguzzi, P. (2007). Detection of a two-photon transition by stimulated emission: Amplification and circular birefringence. *Physical Review A*, *75*(2), 023408.

Sargsyan, A., Bason, M. G., Sarkisyan, D., Mohapatra, A. K., & Adams, C. S. (2010). Electromagnetically induced transparency and two-photon absorption in the ladder system in thin columns of atomic vapors. *Optics and Spectroscopy*, *109*(4), 529–537.

Sargsyan, A., Sarkisyan, D., Krohn, U., Keaveney, J., & Adams, C. (2010). Effect of buffer gas on an electromagnetically induced transparency in a ladder system using thermal rubidium vapor. *Physical Review A*, *82*(4), 045806.

Smith, D. A., & Hughes, I. G. (2004). The role of hyperfine pumping in multilevel systems exhibiting saturated absorption. *American Journal of Physics*, *72*(5), 631–637.

Thoumany, P., Germann, T., Hänsch, T., Stania, G., Urbonas, L., & Becker, T. (2009). Spectroscopy of rubidium Rydberg states with three diode lasers. *Journal of Modern Optics*, *56*(18–19), 2055–2060.

Touahri, D., Acef, O., Clairon, A., Zondy, J. J., Felder, R., Hilico, L., et al. (1997). Frequency measurement of the $5S_{1/2}(F=3)$–$5D_{5/2}(F=5)$ two-photon transition in rubidium. *Optics Communications*, *133*(1), 471–478.

Wielandy, S., & Gaeta, A. L. (1998). Investigation of electromagnetically induced transparency in the strong probe regime. *Physical Review A*, *58*(3), 2500–2505.

Xiao, M., Li, Y. Q., Jin, S. Z., & Gea-Banacloche, J. (1995). Measurement of dispersive properties of electromagnetically induced transparency in rubidium atoms. *Physical Review Letters*, *74*(5), 666–669.